



HAL
open science

Data assimilation and modelling of patient-specific single-ventricle physiology with and without valve regurgitation

Sanjay Pant, Chiara Corsini, Catriona Baker, Tain-Yen Hsia, Giancarlo Pennati, Irene Vignon-Clementel

► **To cite this version:**

Sanjay Pant, Chiara Corsini, Catriona Baker, Tain-Yen Hsia, Giancarlo Pennati, et al.. Data assimilation and modelling of patient-specific single-ventricle physiology with and without valve regurgitation. *Journal of Biomechanics*, 2016, 49 (11), pp.2162-2173. 10.1016/j.jbiomech.2015.11.030 . hal-01240146

HAL Id: hal-01240146

<https://inria.hal.science/hal-01240146>

Submitted on 8 Dec 2015

HAL is a multi-disciplinary open access archive for the deposit and dissemination of scientific research documents, whether they are published or not. The documents may come from teaching and research institutions in France or abroad, or from public or private research centers.

L'archive ouverte pluridisciplinaire **HAL**, est destinée au dépôt et à la diffusion de documents scientifiques de niveau recherche, publiés ou non, émanant des établissements d'enseignement et de recherche français ou étrangers, des laboratoires publics ou privés.

Data assimilation and modelling of patient-specific single-ventricle physiology with and without valve regurgitation

Sanjay Pant^a, Chiara Corsini^b, Catriona Baker^c, Tain-Yen Hsia^c, Giancarlo Pennati^b, Irene E Vignon-Clementel^a, for Modeling of Congenital Hearts Alliance (MOCHA) Investigators¹

^aInria Paris-Rocquencourt & Sorbonne Universités UPMC Paris 6, Laboratoire Jacques-Louis Lions, France

^bLaboratory of Biological Structure Mechanics, Department of Chemistry, Materials and Chemical Engineering 'Giulio Natta', Politecnico di Milano, Italy

^cCardiac Unit, UCL Institute of Cardiovascular Science, and Great Ormond Street Hospital for Children, London, UK

Abstract

A closed-loop lumped parameter model of blood circulation is considered for single-ventricle shunt physiology. Its parameters are estimated by an inverse problem based on patient-specific haemodynamics measurements. As opposed to a black-box approach, maximizing the number of parameters that are related to physically measurable quantities motivates the present model. Heart chambers are described by a single-fibre mechanics model, and valve function is modelled with smooth opening and closure. A model for valve prolapse leading to valve regurgitation is proposed. The method of data assimilation, in particular the unscented Kalman filter, is used to estimate the model parameters from time-varying clinical measurements. This method takes into account both the uncertainty in prior knowledge related to the parameters and the uncertainty associated with the clinical measurements. Two patient-specific cases – one without regurgitation and one with atrioventricular valve regurgitation – are presented. Pulmonary and systemic circulation parameters are successfully estimated, without assumptions on their relationships. Parameters governing the behaviour of heart chambers and valves are either fixed based on biomechanics, or estimated. Results of the inverse problem are validated qualitatively through clinical measurements or clinical estimates that were not included in the parameter estimation procedure. The model and the estimation method are shown to successfully capture patient-specific clinical observations, even with regurgitation, such as double peaked nature of valvular flows and anomalies in electrocardiogram readings. Lastly, biomechanical implications of the results are discussed.

Keywords: single-ventricle physiology, valve regurgitation, data assimilation, unscented Kalman filter, patient-specific modelling, single-fibre heart model

1. Introduction

Lumped parameter models (LPM) are widely employed for assessment of haemodynamics (Shi et al., 2011). They can be either coupled with 3D Navier-Stokes models, for *e.g.* to assist surgical planning (Vignon-Clementel et al., 2010; Baretta et al., 2011; Arbia et al., 2015; Corsini et al., 2014), employed for parameter estimation later used in 3D (Pant et al., 2014), or run independently, for *e.g.* to assess ranges of variation and

Email addresses: Sanjay.Pant@inria.fr (Sanjay Pant), Irene.Vignon-clementel@inria.fr (Irene E Vignon-Clementel)

¹MOCHA investigators: Andrew Taylor, MD, Alessandro Giardini, MD, Sachin Khambadkone, MD, Silvia Schievano, PhD, Marc de Leval, MD, and T.-Y. Hsia, MD (Institute of Cardiovascular Sciences, UCL, London, UK); Edward Bove, MD and Adam Dorfman, MD (University of Michigan, Ann Arbor, MI, USA); G. Hamilton Baker, MD and Anthony Hlavacek (Medical University of South Carolina, Charleston, SC, USA); Francesco Migliavacca, PhD, Giancarlo Pennati, PhD, and Gabriele Dubini, PhD (Politecnico di Milano, Milan, Italy); Alison Marsden, PhD (University of California, San Diego, CA, USA); Jeffrey Feinstein, MD (Stanford University, Stanford, CA, USA); Irene Vignon-Clementel (INRIA, Paris, France); Richard Figliola, PhD and John McGregor, PhD (Clemson University, Clemson, SC, USA)

the effect of functional parameters that are not easily measurable (Hann et al., 2011; Sugimoto et al., 2013). For a patient-specific analysis, however, the LPMs need customisation for each patient individually. While it is natural that the parameters of the LPMs be estimated via some patient-specific clinical measurements such that the discrepancy between model output and the measurements is minimised, the inverse problem is challenging, particularly when the number of parameters to be estimated is high. This phenomenon, often referred to as the *curse of dimensionality* (Bellman et al., 1961), is associated with the exponential increase in the search volume (the volume in the parametric space to be searched for minimising the discrepancy function) with the number of dimensions/parameters. The problem is further exacerbated by uncertainty in the clinical measurements. In principle, a manual tuning of the parameters could be performed, but it is a long process requiring much biomechanical and physiological expertise (see for example, Baretta et al. (2011)). Automatic approaches, on the other hand, are mostly confined to either models with a low number of estimated parameters (for example 6 in Hann et al. (2010) and 2+5+5+2+2 Revie et al. (2013) where five sub-problems are created for the full circulatory model) or open-loop circulatory models with simplified boundary conditions (Arbia et al., 2015; Spilker and Taylor, 2010). Furthermore, such methods typically make inherent hypotheses about the ratios of different parameters (Spilker and Taylor, 2010) or consider only the major model parameters (Sugimoto et al., 2013) to reduce the total number of free parameters. Most commonly a *variational* approach is used to minimise a loss function associated with the discrepancy between the model output and clinical measurements (see for example Hann et al. (2004); Segers et al. (2008); Spilker and Taylor (2010); Ismail et al. (2012); Sugimoto et al. (2013)). Other iterative approaches include fixed-point/control-system based methods (Hann et al., 2010, 2011; Troianowski et al., 2011; Revie et al., 2013; Xiao et al., 2013; Arbia et al., 2015). All these methods usually employ targets of the mean/extrema values or scalar shape descriptors of the clinical measurements and are successful only when a few parameters (in each individual sub-problem if the inverse problem is subdivided) are to be estimated. An alternate approach for parameter estimation that has gained a lot of attention in recent years is the approach of data assimilation. Such approaches are typically based on sequential filtering and take advantage of time-varying measurement curves. These methods have been applied in hemodynamics to estimate tissue/wall material properties or Windkessel parameters (Bertoglio et al., 2012; Moireau et al., 2012; Pant et al., 2014). The first contribution of this manuscript is to present such an approach for parameter estimation in closed-loop models of circulation with many (33) parameters of the heart and circulation.

This study considers single ventricle physiology of both hypoplastic left, and hypoplastic right ventricular aetiology. Specifically, at the time of clinical assessment for planning second stage surgery, whereby clinical, imaging, and pressure data are available for clinical decision-making. Moving from a post stage-I circulation to a stage-II circulation represents a potentially great change in ventricular preload and afterload as the systemic and pulmonary circulations are reconnected. This physiology is described in detail in Corsini et al. (2014). Assessment of patients at this time point is challenging due to both the complex physiology, and the inherent difficulties in acquiring clinical measurements in babies with potentially unstable physiologies. Contrary to the commonly employed time-varying elastance based models for heart function (Mynard et al., 2012; Sugimoto et al., 2013; Shimizu et al., 2010), cardiac chamber (ventricle or atrium) pressure and volume are related to myofibre stress and strain in this study by a one-fibre model of cardiac mechanics (Arts et al., 1991). Note that another lumped model with active and passive components (parameterised from 1D muscle experiments) was derived for the left ventricle (Caruel et al., 2014). The main motivation here is that cardiac biomechanics is described more accurately, for both the ventricle and the atrium, while limiting the number of unknown parameters. Indeed, myofibre passive and active behaviours have been experimentally measured and reported in the literature while other patient-specific parameters (e.g. chamber wall volume) can be individually measured. Consequently, a number of parameters can either be eliminated from the inverse problem, or their estimates can be validated through the measured values. The application of such a model to assess patient-specific cardiac function in this challenging single-ventricle pathophysiology is the second contribution of this study.

The final contribution of this study concerns modelling of heart valves. In single ventricle circulations, atrioventricular valve regurgitation is associated with poor longterm outcome (Honjo et al., 2011a). In these patients the mechanism of regurgitation is likely to be multifactorial. Among lumped parameter models of valves, a pure diode-like behaviour has been adopted where the valve is either entirely open or entirely

closed at any time (Shimizu et al., 2010; Baretta et al., 2011; Corsini et al., 2011) or quite complex models, requiring a large number of parameters, have been used to simulate smooth opening/closure (Korakianitis and Shi, 2006; Paeme et al., 2011). An intermediate simpler approach has been developed by Mynard et al. (2012) describing valve dynamics effectively through few parameters. Nevertheless, in all cases valve regurgitation is simply modelled as due to an incomplete and stable leaflet closure, without accounting for possible valve prolapse. Here, an improvement of the model by Mynard et al. (2012), where valve dynamics is modified to include valve prolapse, is presented. This new model is utilised in single-ventricle physiology and patient-specific valve parameters are estimated.

The above three contributions are tested on two patient-specific cases: one without regurgitation and one with atrioventricular valve (AVV) regurgitation due to prolapse. A large number of parameters (at least 33 per patient) are estimated for each patient from different kind of clinical measurements – magnetic resonance imaging (MRI), Doppler velocimetry, and pressure catheter measurements – with different levels of associated uncertainty. The inverse problem is solved through the data assimilation method of the unscented Kalman filter, and the results are validated qualitatively through measurements that are not used for parameter estimation: Doppler velocimetry measurements of valvular flows, MRI valvular area and ventricular wall and cavity volume measurements, four-chamber echocardiography measurements to derive atrial volumes, and electrocardiography (ECG) measurements for timing of cardiac events.

2. Model and Methods

2.1. Closed-loop model for single-ventricle physiology

The closed-loop model for single-ventricle physiology is depicted in Figure 1. The four districts of circulation – the heart, upper body, lower body, and the lungs – are lumped individually. Owing to the atrial septal defect the two chambers are considered as a single atrium (SA). The SA is connected via the AVV to the single ventricle (SV) which in turn feeds into the systemic circulation via the aortic valve (AOV). The connection between the systemic and pulmonary circulations is made via a systemic-to-pulmonary artery shunt (SH) that connects the aorta to the pulmonary artery. The systemic and pulmonary districts are described in a similar manner (except for inclusion of shunt in the Lung district) through a series of elements representing linear viscous losses (R), quadratic viscous losses (K), blood inertia (L), and vessel wall compliances (C). In Figure 1, similar to Baretta et al. (2011), the large arteries (with subscript 1), small vessels (with subscript 2), and veins (with subscript 3) are distinctly represented. An algebraic and ODE system describing the model haemodynamics can be written. The pressure-flow relationships followed by R , K , L and C components are shown in Table 1, while sections 2.2 and 2.3 describe the heart and valve models. Lastly, mass balance at every node of Figure 1 completes the ODE system.

2.2. Single fibre model for a heart chamber

A heart chamber (SA or SV) is described by a single fibre wrapped around the cavity (Arts et al., 1991, 2003; Bovendeerd et al., 2006). This model is particularly suitable for lumped modelling as it was shown that under rotational symmetry the shape of the chamber and other geometric parameters had little effect on the relationship between the cavity pressure and fibre stress (Arts et al., 1991). This relationship is dominated by the ratio of the cavity volume V to wall volume V_w (volume of the cavity wall), and is given by

$$\frac{\sigma_f}{P} = \left(1 + \frac{3V}{V_w} \right) \quad (1)$$

where P represents the pressure of the chamber and σ_f is the stress in the fibre. The fibre stress is composed of two components: an active component σ_a and a passive component σ_p

$$\sigma_f = \sigma_a + \sigma_p \quad (2)$$

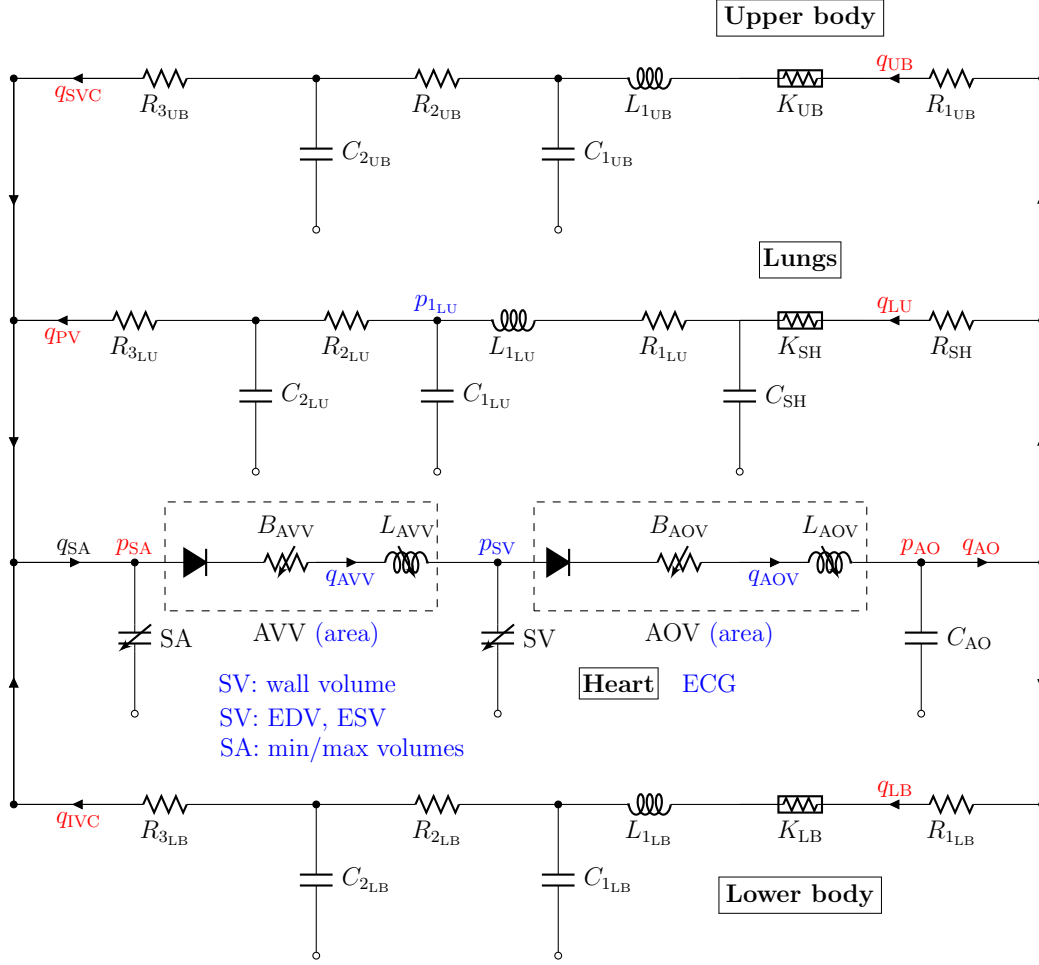


Figure 1: Schematic of a closed-loop model for single-ventricle circulation. The heart components are derived in sections 2.2 and 2.3. For description of other components see table 1. The measurements for parameter estimation are shown in red, while the measurements for validation are shown in blue.

If V_0 and l_0 represent the state of the cavity and sarcomere length, respectively, at zero transmural pressure, then at a general state of cavity volume V , the sarcomere length, l , can be written as

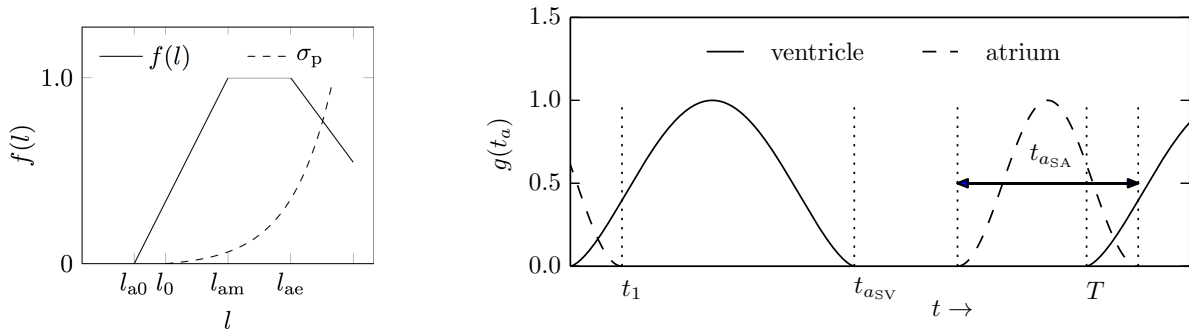
$$\frac{l}{l_0} = \lambda = \left(\frac{1 + (3V/V_w)}{1 + (3V_0/V_w)} \right)^{1/3} \quad (3)$$

where λ is the fibre stretch ratio. The sarcomere shortening velocity, v_s , is given by

$$v_s = -\frac{dl}{dt} = -\frac{l}{V_w} \left(1 + \frac{3V}{V_w} \right)^{-1} \frac{dV}{dt} \quad (4)$$

The active component of the stress is described as

$$\sigma_a = T_{a0} f(l) g(t_a) h(v_s) \quad (5)$$



(a) Sarcomere active and passive stress (σ_p not to scale).

(b) Activation curves for the atrium and ventricle: T : cardiac cycle; t_{\max} of equation (7): t_{aSV} for the ventricle and t_{aSA} for the atrium; and t_1 : overlap between atrium and ventricle activations.

Figure 2: Sarcomere properties and chamber activation functions

$$f(l) = \begin{cases} 0, & \text{if } l < l_{a0} \\ (l - l_{a0}) / (l_{am} - l_{a0}), & \text{if } l_{a0} < l \leq l_{am} \\ 1.0, & \text{if } l_{am} < l \leq l_{ae} \\ (l_{af} - l) / (l_{af} - l_{ae}), & \text{if } l > l_{ae} \end{cases} \quad (6)$$

$$g(t_a) = \begin{cases} \left[\frac{1}{2} \left(1 - \cos \left(2\pi \frac{t_a}{t_{\max}} \right) \right) \right]^{E_a}, & \text{if } t_a < t_{\max} \\ 0, & \text{otherwise} \end{cases} \quad (7)$$

$$h(v_s) = \frac{1 - (v_s/v_0)}{1 + c_v (v_s/v_0)} \quad (8)$$

where t_a is the time since activation of the cavity, t_{\max} is the total time of activation in a cardiac cycle, v_0 is the initial sarcomere shortening velocity, T_{a0} is the maximum active sarcomere stress, and c_v is a shape parameter. The functions $f(l)$ and $g(t_a)$ are shown in Figure 2. Note that the function $g(t_a)$ is parameterised to allow for overlaps between the atrial and ventricular contractions. The passive stress is given by

$$\sigma_p = \begin{cases} 0, & \text{if } \lambda < 1 \\ T_{p0} (\exp \{c_p(\lambda - 1)\} - 1), & \text{if } \lambda \geq 1 \end{cases} \quad (9)$$

where T_{p0} and c_p are sarcomere material constants. The relationship between P , V , and dV/dt of a heart-chamber is thus given by equations (1) – (9).

2.3. A model for valve function

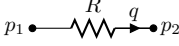
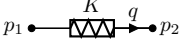
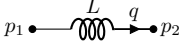
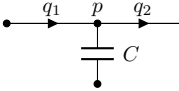
Valve regurgitation may be associated to either an incomplete closure of the valve leaflets or due to valve prolapse (Honjo et al., 2011a,b). For valve function, the model proposed in Mynard et al. (2012) is modified to include the latter. For a fluid with density ρ , the pressure drop across a valve is described by the Bernoulli relation

$$\Delta p = Bq|q| + L \frac{dq}{dt} \quad (10)$$

$$B = \frac{\rho}{2A_{\text{eff}}^2} \quad \text{and} \quad L = \frac{\rho l_{\text{eff}}}{A_{\text{eff}}} \quad (11)$$

where A_{eff} and l_{eff} are the effective area and effective length of the valve, respectively. Note that, the viscous losses are small and thus neglected (Mynard et al., 2012; Sun et al., 1995). The valve state can be described

Table 1: Pressure and flow-rate relationship for various components: p represents pressure and q represents flow-rate

Component	pressure-flow relationship	Component	pressure-flow relationship
	$p_1 - p_2 = R q$		$p_1 - p_2 = K q q $
	$p_1 - p_2 = L \dot{q}$		$q_1 - q_2 = C \dot{p}$

by a single variable, $\xi(t)$, which in turn depends on the pressure difference across the valve, $\Delta p = p_{\text{up}} - p_{\text{down}}$ (e.g. $p_{\text{up}} = p_{\text{SA}}$ and $p_{\text{down}} = p_{\text{SV}}$ for AVV). The dependence of the valve effective area on $\xi(t)$ is different according to valve condition, namely:

$$A_{\text{eff}}(t) = \begin{cases} A_{\text{eff}}^{\text{max}} \xi(t) & \text{if valve is not regurgitant} \\ A_{\text{eff}}(t) = (A_{\text{eff}}^{\text{max}} - A_{\text{eff}}^{\text{min}}) \xi(t) + A_{\text{eff}}^{\text{min}} & \text{if valve is regurgitant due to incomplete leaflet closure} \\ \begin{cases} A_{\text{eff}}^{\text{max}} \xi(t) & \text{if } \xi \geq 0 \\ -A_{\text{eff}}^{\text{r,max}} \xi(t) & \text{if } \xi < 0 \end{cases} & \text{if valve is regurgitant due to prolapse} \end{cases} \quad (12)$$

Generally, $\xi(t)$ varies between -1 and +1. In the first two cases $\xi(t)$ is always positive, whereas in the prolapse case it can become negative. Note that the maximum number of parameters to identify is two.

Four dynamic valve states are taken into account, namely i) opening, ii) closing, iii) prolapse increasing, and iv) prolapse decreasing:

$$\begin{cases} \dot{\xi} = (1 - \xi) K_{\text{vo}} \Delta p & \text{if } \Delta p \geq 0 \\ \dot{\xi} = \xi K_{\text{vc}} \Delta p & \text{if } \Delta p_{\text{rg}} \leq \Delta p < 0 \text{ and } \xi \geq 0 \\ \dot{\xi} = (1 + \xi) K_{\text{vo}}^{\text{r}} (\Delta p - \Delta p_{\text{rg}}) & \text{if } \Delta p \leq \Delta p_{\text{rg}} \\ \dot{\xi} = -\xi K_{\text{vc}}^{\text{r}} (\Delta p - \Delta p_{\text{rg}}) & \text{if } \Delta p > \Delta p_{\text{rg}} \text{ and } \xi < 0, \end{cases} \quad (13)$$

where K_{vo} , K_{vc} , K_{vo}^{r} , and K_{vc}^{r} are the proportionality rates.

If the valve does not prolapse, only the first two equations hold. When $\xi(t)$ is zero, the valve is closed. It is assumed that valve starts to open when $\Delta p > 0$ and starts to close when $\Delta p < 0$. Prolapse starts when $\Delta p < \Delta p_{\text{rg}}$, assuming that valvular structures (e.g. chordae tendineae) cannot maintain a competent valve for excessive negative Δp .

2.4. Data assimilation for parameter estimation

Data assimilation refers to the process of merging numerical model predictions with available measurements to provide an improved estimate of the dynamical system (Bertagna et al., 2014). It is well suited for a patient-specific analysis, since the mathematical description is combined with clinical measurements. For the choice of unscented Kalman filter (UKF) for data assimilation, its appropriateness for parameter estimation in non-linear systems, and application to haemodynamics, Pant et al. (2014) is referred. The method is now briefly described. Consider a dynamical system described by state variables $\mathbf{x} \in \mathbb{R}^d$, $\mathbf{x} = [x_1, x_2, \dots, x_d]^T$ and parameterised by $\boldsymbol{\theta} \in \mathbb{R}^p$, $\boldsymbol{\theta} = [\theta_1, \theta_2, \dots, \theta_p]^T$, with following dynamics

$$\mathbf{x}_{n+1} = F(\mathbf{x}_n, \boldsymbol{\theta}), \quad (14)$$

where \mathbf{x}_n and \mathbf{x}_{n+1} refer to the state at times t_n and t_{n+1} . Equation (14) can, for example, be considered as a discretised form of the ODE system $\dot{\mathbf{x}} = \mathcal{F}(\mathbf{x}, \boldsymbol{\theta})$. Consider that at time t_n , measurements of vector

$\mathbf{y} \in \mathbb{R}^m$, $\mathbf{y} = [y_1, y_2, \dots, y_m]^T$ are available and related to the state through the observation operator H and measurement noise ϵ as follows

$$\mathbf{y}_n = H(\mathbf{x}_n) + \epsilon_n. \quad (15)$$

In the above, the noise at all measurement times is assumed to be independent and distributed according to a multivariate Gaussian distribution with zero mean and covariance Σ_n . The goal of all filtering methods is to provide estimates of \mathbf{x}_n recursively at each measurement time t_n through the measurements \mathbf{y}_n . This is achieved through two steps of propagation and correction. Assume that an estimate of state is available at time t_n with mean $\hat{\mathbf{x}}_n$ and covariance \mathbf{P}_n . The forward propagation step involves propagation of the mean and covariance from t_n to t_{n+1} through the forward model of equation (14). In the correction step, these means and covariances are corrected through the measurement of \mathbf{y}_{n+1} to yield an estimate of mean $\hat{\mathbf{x}}_{n+1}$ and covariance \mathbf{P}_{n+1} at t_{n+1} . Thus, starting from an initial estimate of the state with mean \mathbf{x}_0 and covariance \mathbf{P}_0 , an estimate of the state is available at all times through the filter. Parameter estimation is performed by considering an augmented state containing the parameters $\mathbf{z}_n = [\mathbf{x}_n, \boldsymbol{\theta}_n]^T$ and adding trivial dynamics $\dot{\boldsymbol{\theta}} = 0$, *i.e.* $\boldsymbol{\theta}_{n+1} = \boldsymbol{\theta}_n$, for the parameters in equation (14). The filter is run on the augmented state \mathbf{z} , and the $\boldsymbol{\theta}$ component of filtered \mathbf{z} at the last measurement time is taken as the final parameter vector estimate (Pant et al., 2014). The estimate of the parameters depends on three factors: a) the manner in which the parameters affect the measured quantities, *i.e.* the operators F and H in equations (14) and (15); b) the uncertainty associated with prior knowledge about the parameters and the state, *i.e.* \mathbf{x}_0 and \mathbf{P}_0 ; and c) the uncertainty associated with the clinical measurements, *i.e.* \mathbf{y}_n and Σ_n . As a general rule for parameter estimation, the prior variances in \mathbf{P}_0 are set to relatively higher values compared to the variances in Σ_n to imply that initial guess of $\mathbf{z}_0 = [\mathbf{x}_0, \boldsymbol{\theta}_0]^T$ has less confidence when compared to the measurements (Pant et al., 2014).

2.5. Patient-specific cases

Two patient-specific cases (pre stage-II single ventricle shunt physiology) are considered. Institutional Review Board approval and consent from guardians were obtained. Both patients underwent MRI, cardiac catheterization, and trans-thoracic echocardiography for pre-stage-II surgical planning at the routine point of pre-operative assessment (see Appendix).

Patient-A, 3 months old with a body surface area (BSA) of 0.26 m², has a hypoplastic right ventricle due to tricuspid and pulmonary atresia. The representative heart rate is 116 beats per minute (bpm) and there is no valve regurgitation as assessed by MRI and echocardiography. Stage 1 surgery was a 4mm right modified Blalock-Taussig shunt. Patient-B, 5 months old with a BSA of 0.34 m², has a hypoplastic left ventricle due to aortic atresia and mitral hypoplasia. Stage 1 surgery was a 3.5mm right modified Blalock-Taussig shunt. The representative heart rate is 140 bpm and an AVV regurgitation fraction of 25 % is measured by MRI.

For both the patients, the ODE system for the forward model and the UKF are implemented in-house in the Python programming language (with Cython compiler) using the modules NumPy, SciPy, and multiprocessing (for a parallel propagation of Sigma-points in the UKF). All simulations are run on an HPC node (RAM 48 GB) with 2 Intel Xeon X5650 processors, each with 6 cores and 12 threads. In this setting, with 20 parallel processes the UKF takes around 140 seconds to assimilate observations at 200 discrete time instants in one cardiac cycle.

2.6. Parameters to be estimated and available measurements

An advantage of the mechanics-based heart model is that the sarcomere material parameters need not be estimated. Consequently, these are kept fixed to literature values (Beyar and Sideman (1984); Bovendeerd et al. (2006)), see Table 2. The activation functions are governed by three parameters (see Figure 2b): $t_{a_{SV}}$ and $t_{a_{SA}}$, the ventricle and atrium activation durations, respectively, and t_1 , a small overlap between them. For both patients, $A_{\text{eff}}^{\text{min}}$ is set to zero. Thus, for patient-A with no AVV regurgitation only $A_{\text{eff}}^{\text{max}}$, and for patient-B $A_{\text{eff}}^{\text{max}}$ and $A_{\text{eff}}^{\text{r,max}}$, need to be estimated. The opening and closing rate constants are fixed to those reported for different valves in Mynard et al. (2012). In absence of empirical measures for regurgitant valves, these rates are considered normal in the regurgitation model. Lastly, the shunt parameters R_{SH} and K_{SH}

Table 2: Reference values for sarcomere material behaviour

Parameter	Value	Parameter	Value	Parameter	Value
l_0	1.9 μm	l_{ae}	2.4 μm	T_{a0}	55 kPa
l_{a0}	1.65 μm	v_0	10 $\mu\text{m/s}$	T_{p0}	0.9 kPa
l_{am}	2.2 μm	c_p	12	c_v	0

are fixed according to shunt diameter (Migliavacca et al., 2000). The identified parameters are summarised in Table 3.

For parameter estimation the following measurements (see Figure 1 labels in red) are used for patient-A: pressure catheter measurements of p_{SA} and p_{AO} ; MRI flow-rate measurements for q_{AO} , q_{LB} , q_{PV} , q_{IVC} , and q_{SVC} ; measurement curve for q_{LU} constructed through Doppler velocimetry measurements of shunt flow and the findings of Migliavacca et al. (2000); and q_{UB} obtained via mass balance. For patient-B, an identical set is used, except that q_{LB} is based on Doppler velocimetry in absence of MRI measurement.

For validation, the following measurements are used (see Figure 1 labels in blue): pressure catheter p_{SV} , Doppler velocimetry measurements q_{AVV} and q_{AOV} , the pulmonary venous wedge pressure, MRI SV wall volumes, atria areas in the four-chamber echocardiography view, and ECG measurements.

3. Results and discussion

3.1. Patient-A

The parameters evolution by the UKF is shown in Figure 3. From an initial guess, the UKF continuously corrects the parameters until convergence (stabilisation) such that the time-curves of the provided measurements are closely reproduced. Their final estimates are shown in Table 3. Model predictions and the clinical measurements are compared in Figure 4. Pressure in the single-ventricle is presented for qualitative validation as it is not provided to the UKF for parameter estimation. The mean flow-rates in the model, though not explicit targets in the UKF, have 5% maximum errors compared to the clinical measurements. Pressure drop in any systemic district occurs primarily in small-vessels/capillaries. This is reflected correctly in the parameter estimates where in each district the resistance R_2 (reflecting pressure drop in the small vessels) is higher than both R_1 and R_3 (reflecting pressure drop in the arteries and veins). Comparing pulmonary venous wedge pressure measurements (Figure 5a) to p_{1LU} time-tracings in Figure 4 shows a good agreement in its range of variation. The model is further validated by valvular flows. Comparing q_{AVV} in model predictions of Figure 4 to its velocimetry measurements in Figure 5b it is observed that the double-peak structure is reproduced in the model. Similarly, for q_{AOV} , Figure 5c shows a small but clearly identifiable back-flow during valve-closure (end of ventricular systole), which is reproduced in the model. These observations and validation for valvular flow-rates are particularly encouraging as they are a result of the smooth opening/closure model. The commonly employed ideal-diode model cannot reproduce such physiological flow-rates.

As mentioned above, the heart model was chosen for its parameters physical interpretation and possible direct measurement. For example the measured SV wall volume is 34.2 ml. Its estimation is 33.9 ml, and provides further confidence in both the model and the parameter estimation method. Similarly, at a higher heart-rate of 136 bpm, MRI ventricular volumes were measured to be 29 ml and 10 ml at end diastole and end systole, respectively. In the model, at a heart-rate of 116 bpm, these vary between 24.5 ml and 10.7 ml, which is in good agreement with the measurements given that the heart rate, and hence stroke volume, is higher. The atrium volume measurement is more difficult. A rough clinical estimate can, however, be obtained via area measurements through echocardiography four-chamber view. The right and left atria areas are measured to vary from 3.0–4.5 cm^2 and 2.0–2.5 cm^2 , respectively. Under the simplification of spherical geometry, the combined volume is estimated to vary from 6.03 ml to 10.15 ml. In the model it varies between 8.1 ml and 15.5 ml, which agrees reasonably with the rough clinical estimates.

The MRI reconstructed AVV and AOV annulus areas are 2.8 cm^2 and 2.0 cm^2 . These measurements are also consistent with MRI measurements of the maximum orifice area (leaflet opening area). In the

model, the maximum effective area reflects directly neither the annulus area nor the leaflet area, but the maximum area of the jet-flow across the valve. One way to convert the area at leaflet level to the jet area is to consider hydraulic constants, which can result in the jet area being smaller than the leaflet area by factors between 0.4 and 0.7 (Segal et al., 1987). A comparison of the model predictions to the maximum leaflet area measurements yields a factor of 0.4 and 0.785 for the AVV and AOV, respectively.

3.2. Patient-B

Patient-B is a particularly challenging paediatric case to model, not only due to the presence of 25% AVV regurgitation, but also due to higher aortic pressures (~ 120 mmHg) and highly oscillating venous flows. For example, while the measured IVC mean-flow is 3 ml/s, it oscillates between ± 100 ml/s during the cardiac cycle. Furthermore, the available pressure measurements and MRI flow-rates were acquired at different heart rates of 106 bpm and 140 bpm, respectively. Lastly, the flow-rates q_{LB} and q_{UB} are constructed via Doppler velocimetry and consequently their time-variation needs to be accounted with care. In the UKF method this is achieved by providing a relatively higher measurement error variance for these measurements in comparison to those for the MRI flow-rates.

For patient-B, the regurgitant area $A_{\text{effAVV}}^{r,\text{max}}$ needs to be additionally estimated. Δp_{rg} is fixed to -50 mmHg based on numerical experiments. A first parameter estimation, while successfully reproducing the measurements closely, yielded an abnormally high ventricle wall volume (130 ml). On further examination, for the measured wall volume of 40 ml and the measured end systolic volume of 13 ml, the passive stress behaviour of equation (9) with reference values of $T_{p0} = 0.9$ and $c_p = 12$, yields a ventricular end diastolic pressure (EDP) of ~ 18 mmHg. The EDP in the patient was measured to vary from 4–8 mmHg (it usually varies from 0–7 mmHg in normal adults (Berne and Levy, 1967)) implying that the passive stress in the ventricle is overestimated. This could be due to ventricular remodelling or due to the difference between passive behaviour of the right and left ventricles (Moskowitz, 1982). Note that the reference values for the passive behaviour are based on myocardium strips obtained from left ventricles and patient-B has a functioning right ventricle.

Having established that the passive behaviour needs to be estimated for patient-B, another UKF estimation is performed where the ventricle wall volume is fixed to 40 ml and the parameter T_{p0} governing passive behaviour, see equation (9), is estimated. The parameters evolution in the UKF in Figure 6 show good convergence to their final estimates (Table 3). The model outputs compare well with the measurements in Figure 7. The AVV behaviour is modelled as expected for valve prolapse (ξ_{AVV} goes to -1 during ventricular systole). Consequently, q_{AVV} is negative in this time-interval, with mean regurgitation flow of 10.3 ml/s (measured: 10.5 ml/s). The cardiac output is 41.0 ml/s compared to the measured value of 41.5 ml/s (calculated via end diastolic and end systolic volumes both in the model and the measurements). This leads to a regurgitation fraction of 22.7 % compared to the measurement of 25.3 %. The model thus reasonably captures the global features of AVV regurgitation.

In Figure 7, all time-varying measurements provided to the UKF are reasonably well reproduced by the model given the aforementioned high uncertainties in some flow-rate measurements and their inconsistency with pressure measurements. In comparison to patient-A, the double-peaked nature of atrial pressure is less pronounced in patient-B (see Figures 4 and 7) in both the measurements and the model outputs. This is likely due to regurgitant flow from the ventricle to the atrium which raises its volume, and consequently its pressure, during this period for patient-B. As for patient-A, the range of variation of p_{LU} , reflective of pulmonary artery pressure in the model, is consistent with the range of variation in the measurements of pulmonary venous wedge pressure (Figures 7 and 8a).

The activation durations $t_{a_{\text{SA}}}$ and $t_{a_{\text{SV}}}$ relative to the cardiac time-period (0.51 s for patient-A and 0.43 s for patient-B) are higher in patient-B than patient-A, see Table 3. In fact these estimates suggest that the atrium activation starts before the end of ventricular activation, see Figure 2b. While seemingly odd, this behaviour is observed clinically: Figure 8b shows an abnormal ECG reading for this patient where the T-wave is merged with the P-wave of the next cardiac cycle. This agreement is very encouraging for both the model and parameter estimation method.

Volume variation of the atrium is higher in patient-B. This is reasonable, as clinically an enlarged right atrium is observed. In the four-chamber view, the left and right atrium areas vary between 1.86–2.73 cm²

Table 3: Parameters estimated by the UKF. The numbers in parenthesis are fixed parameters

Parameter	Estimate (patient-A)	Estimate (patient-B)	unit
V_{0SA}	6.37	11.41	ml
V_{wSA}	1.30	2.55	ml
V_{0SV}	12.4	10.84	ml
V_{wSV}	33.9	(40)	ml
$A_{\text{eff}AVV}^{\text{max}}$	1.10	2.64	cm ²
$A_{\text{eff}AOV}^{\text{max}}$	1.57	0.92	cm ²
$A_{\text{eff}AVV}^{\text{r,max}}$	-	0.036	cm ²
C_{AO}	4.6E-02	2.2E-02	ml/mmHg
R_{1LB}	1.08	3.42	mmHg.s/ml
R_{2LB}	6.62	15.24	mmHg.s/ml
R_{3LB}	0.18	0.044	mmHg.s/ml
K_{LB}	5.0E-03	0.03	mmHg.s ² /ml ²
L_{1LB}	0.027	5.5E-03	mmHg.s ² /ml
C_{1LB}	0.14	0.045	ml/mmHg
C_{2LB}	3.09	3.35	ml/mmHg
R_{1UB}	0.60	0.40	mmHg.s/ml
R_{2UB}	3.26	6.50	mmHg.s/ml
R_{3UB}	0.76	0.16	mmHg.s/ml
K_{UB}	3.3E-03	1.97E-02	mmHg.s ² /ml ²
L_{1UB}	4.0E-04	1.06E-02	mmHg.s ² /ml
C_{1UB}	0.11	0.10	ml/mmHg
C_{2UB}	0.12	0.30	ml/mmHg
R_{1LU}	7.9E-03	0.11	mmHg.s/ml
R_{2LU}	0.54	0.21	mmHg.s/ml
R_{3LU}	0.23	0.08	mmHg.s/ml
L_{1LU}	0.40	0.045	mmHg.s ² /ml
C_{1LU}	0.11	0.11	ml/mmHg
C_{2LU}	0.06	0.64	ml/mmHg
C_{SH}	1.0E-04	0.02	ml/mmHg
E_{aSA}	1.42	1.72	-
E_{aSV}	0.50	0.48	-
t_{aSA}	0.15	0.26	s
t_{aSV}	0.31	0.32	s
t_1	0.05	0.04	s
T_{p0}	(0.9)	0.15	kPa

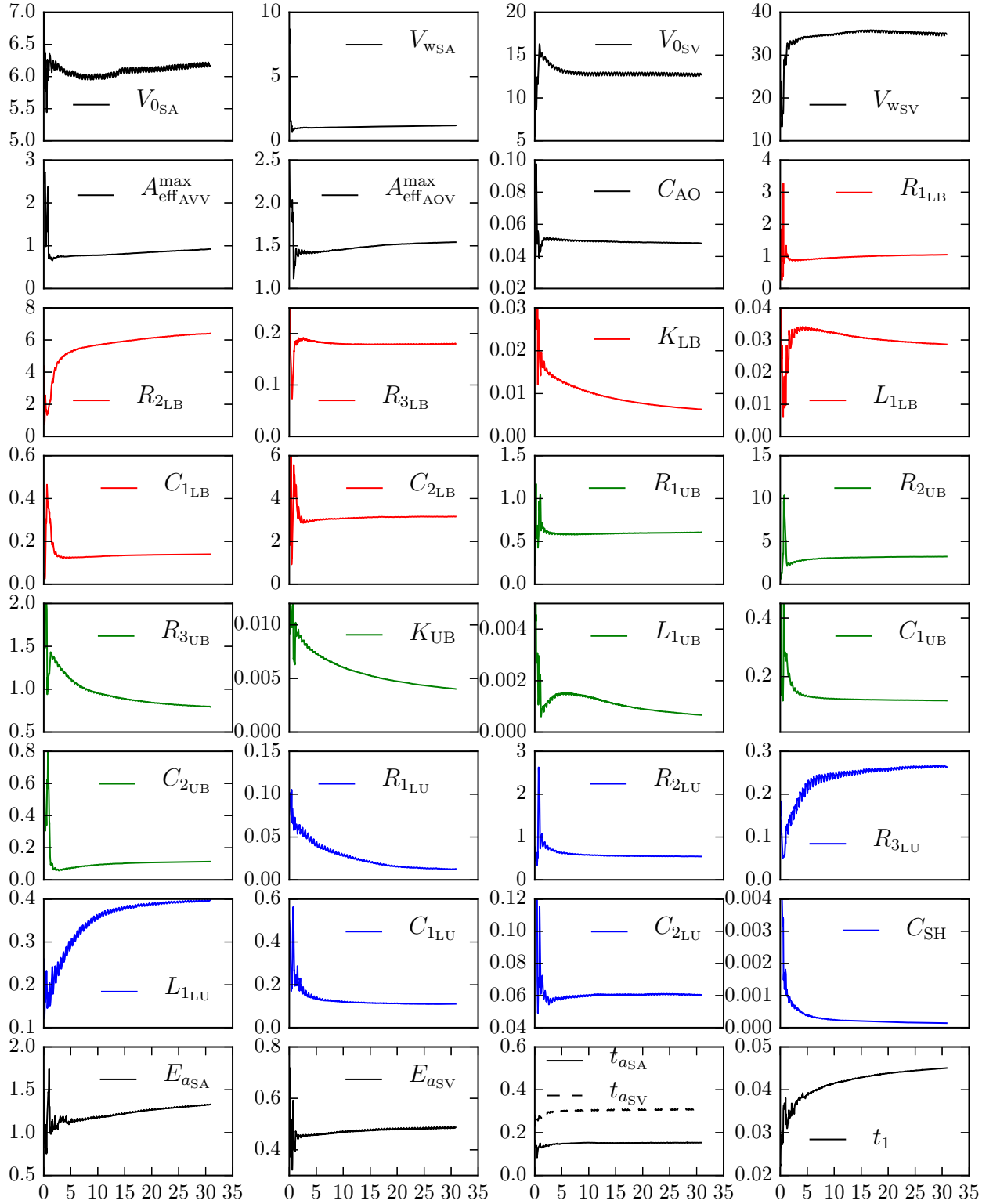


Figure 3: Parameter evolution with UKF for patient-A: time in x-axis (50 cardiac cycles); volumes are in ml; areas (A) are in cm^2 ; linear resistances (R) are in $\text{mmHg}\cdot\text{s}/\text{ml}$; quadratic resistances (K) are in $\text{mmHg}\cdot\text{s}^2/\text{ml}^2$; compliances (C) are in ml/mmHg ; inductances (L) are in $\text{mmHg}\cdot\text{s}^2/\text{ml}$; and time is in s.

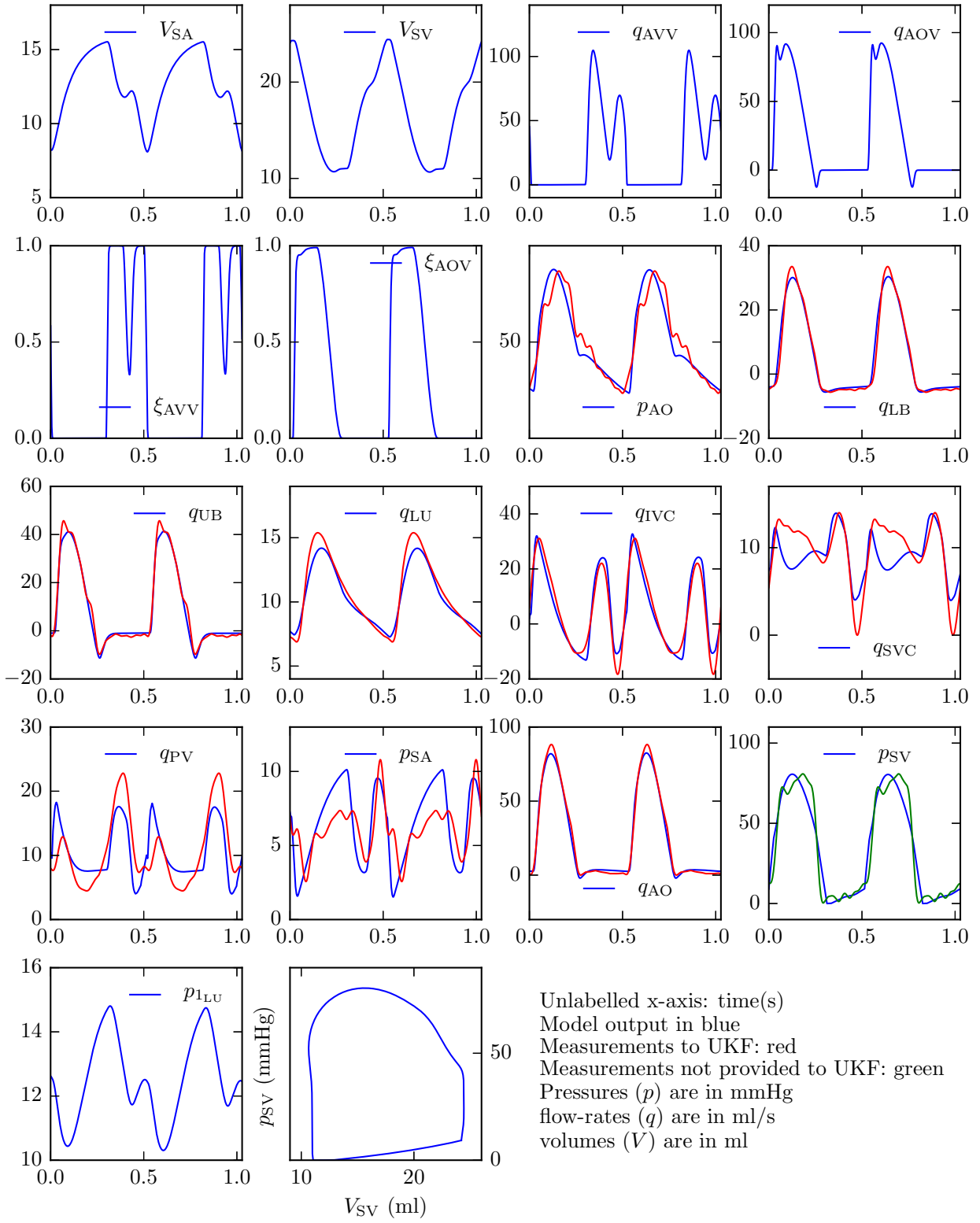


Figure 4: Forward model for patient-A with the estimated parameters: comparison with measurements over two cardiac cycles

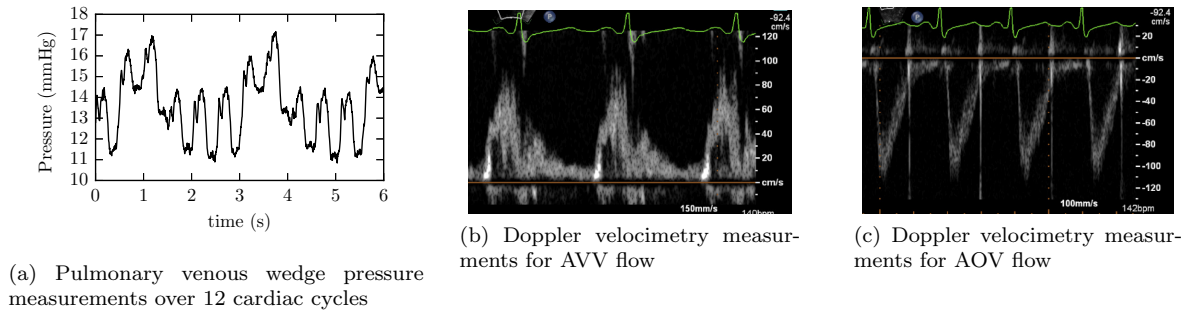


Figure 5: Validation measurements for patient-A

and $6.52\text{--}8.24\text{ cm}^2$, respectively, yielding a combined volume variation of $14.4\text{--}21.2\text{ ml}$. This is consistent with the model output ($9.0\text{--}23.6\text{ ml}$). For the ventricle, the measured end systole and end diastole volumes, 13 and 30 ml , respectively are in good agreement with the model ($12.7\text{--}30.3\text{ ml}$).

Considering hydraulic coefficients (see previous section) yields a factor of 0.98 and 0.45 between the jet-area and the maximum leaflet area of the AVV for normal and regurgitant flow, respectively. This factor for the AOV is 0.38 . All mean flow-rate measurements and model outputs differ by less than 5% , except for q_{IVC} where the error is 15% (model: 3.45 ml/s ; measured: 3.0 ml/s). Recall that this flow oscillates between $\pm 100\text{ ml/s}$. Nevertheless, the time variation is actually well reproduced by the model (see Figure 7). Including exact mean-flow rate measurements in the UKF can easily be implemented through constraints (Pant et al., 2014), but is avoided here owing to measurements uncertainties, particularly for highly oscillatory flows.

Overall, the UKF method is able to successfully estimate 33 and 34 parameters for patients A and B, respectively. In both cases, the results are in good agreement with clinical observations. It should be noted that the UKF is sensitive to the initial guesses and associated variances for the state and the parameters (c.f. Pant et al. (2014)). In this light, a reasonable choice of the initial conditions based on model physics and prior knowledge is important.

4. Conclusion

A lumped parameter network for single-ventricle shunt physiology, with physiologically meaningful heart-model parameters, is presented. In addition, a new model for regurgitation due to valve prolapse with smooth opening and closure of the valves is proposed. It is tested for the tricuspid valve but can be used for other heart valves both in the paediatric and adult populations. Data-assimilation method for estimating a large number of parameters from time-varying clinical measurements is successfully tested. Even though a large number of parameters is estimated, no assumptions regarding the usually employed relationships between the parameters is enforced. This method is applied to two patient-specific cases to estimate the model parameters such that the clinical measurements are well-reproduced in the model. For the patient with atrioventricular valve regurgitation, the measured regurgitation fraction of 25% is well reproduced by the model. The results are further validated by easily measurable and mostly non-invasive clinical measurements such as Doppler velocimetry, ECG, and echocardiography. The model and the parameter estimation method are shown to capture clinical observations such as double-peaks in valvular flows and anomalies in atrial and ventricular contraction durations. The presented models and method can be used in surgical planning, for example in a 3D-LPN coupled haemodynamic studies, or for assessment of functional parameters that are not easily measurable. Furthermore, in a pure LPN setting the effects of increasing heart rate, worsening of regurgitation, etc., can be examined and compared between patients. Lastly, while the patient-specific cases of single-ventricle physiology are presented in this study, the method of parameter estimation is applicable to other physiologies provided a model and enough measured targets are available.

Acknowledgements

This work was supported by the Leducq Foundation as part of the Transatlantic Network of Excellence for Cardiovascular Research “Multi-scale modeling of single ventricle hearts for clinical decision support” and a British Heart Foundation Clinical Research Fellowship FS/12/35/29566.

Conflict of interest

The authors have no conflict of interest related to the work presented in this manuscript.

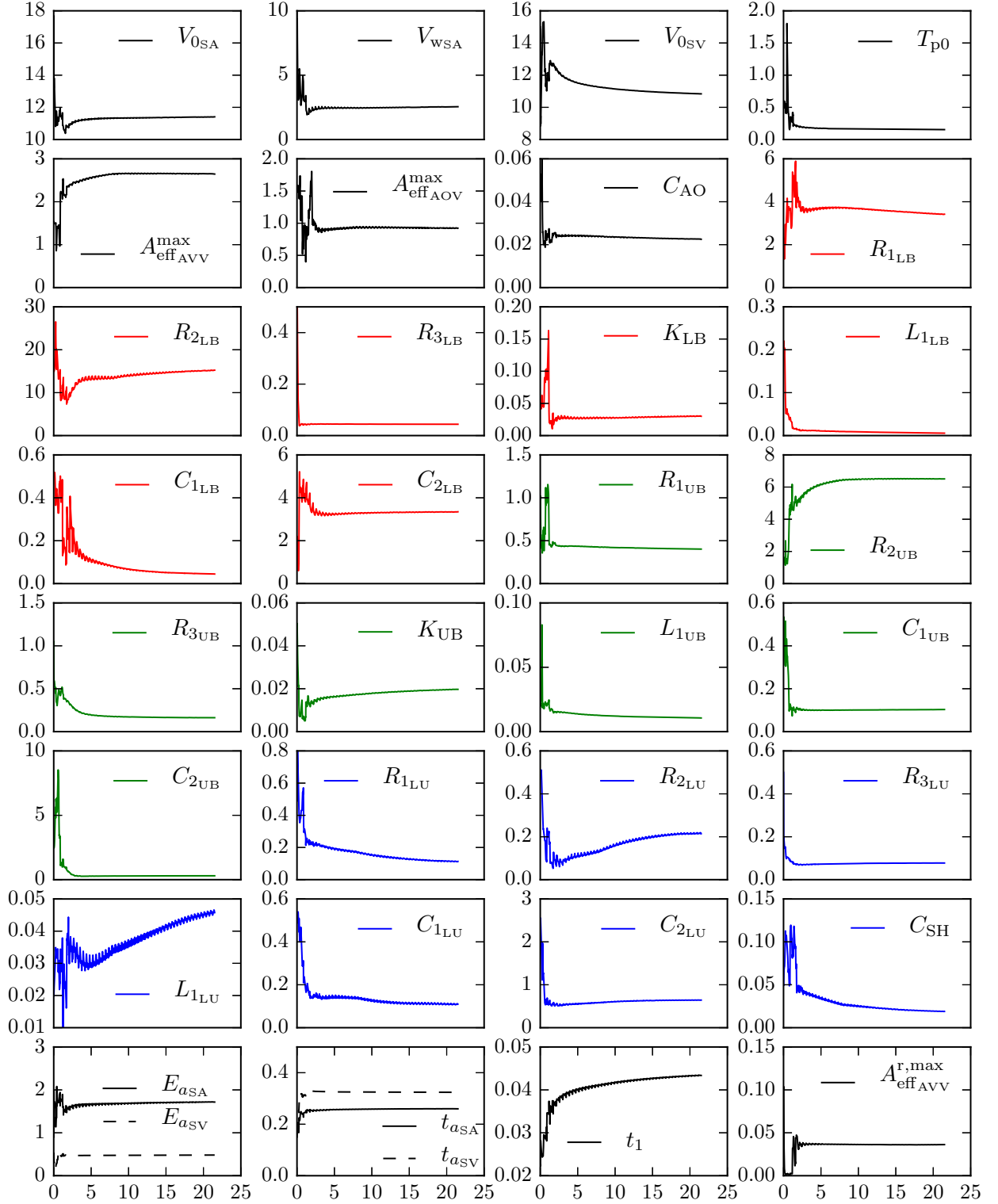


Figure 6: Parameter evolution with UKF for patient-B: time in x-axis (50 cardiac cycles); volumes are in ml; areas (A) are in cm^2 ; linear resistances (R) are in $\text{mmHg}\cdot\text{s}/\text{ml}$; quadratic resistances (K) are in $\text{mmHg}\cdot\text{s}^2/\text{ml}^2$; compliances (C) are in ml/mmHg ; inductances (L) are in $\text{mmHg}\cdot\text{s}^2/\text{ml}$; stress (T_{p0}) is in kPa; and time is in s. Δp_{rg} is fixed at -50 mmHg.

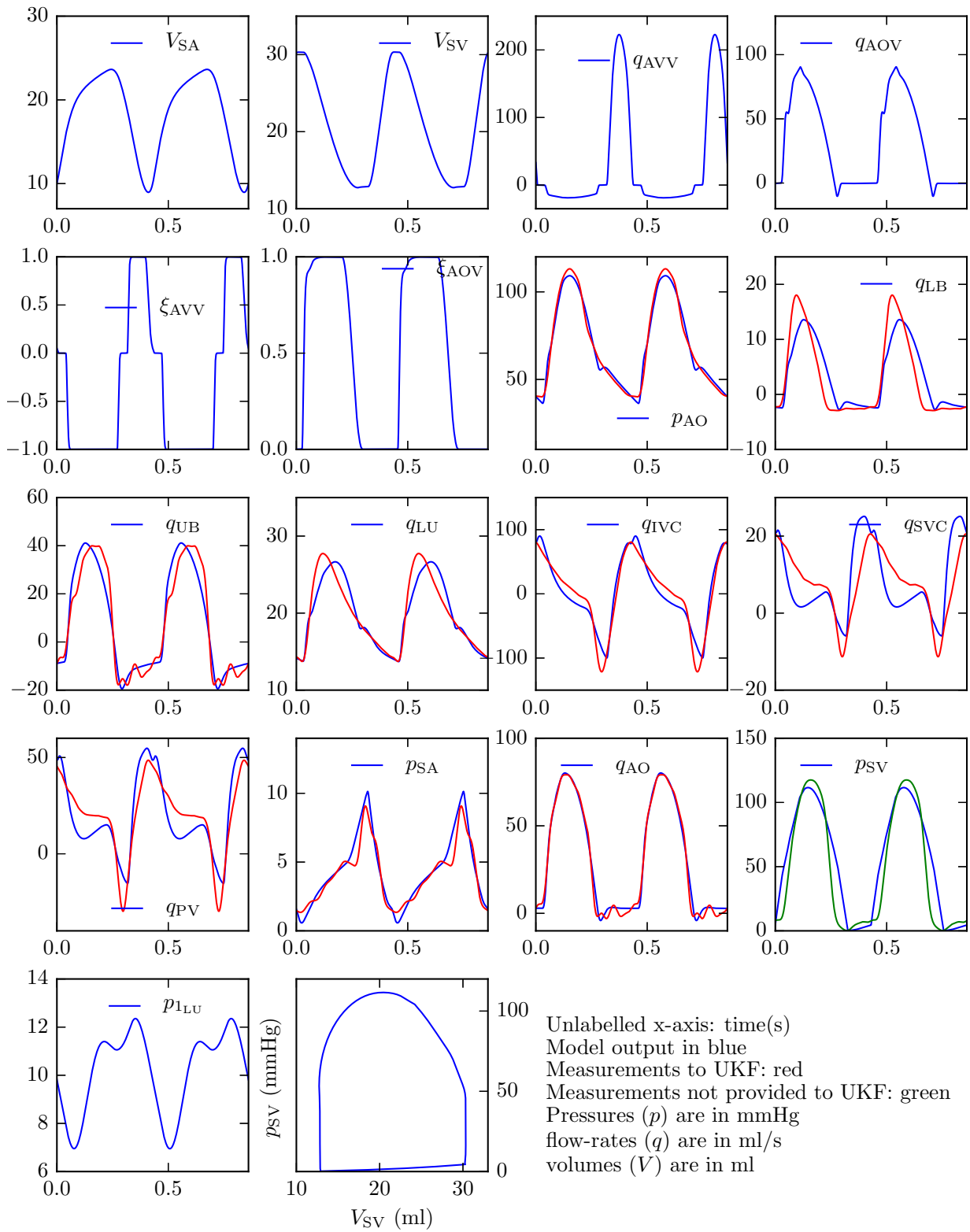
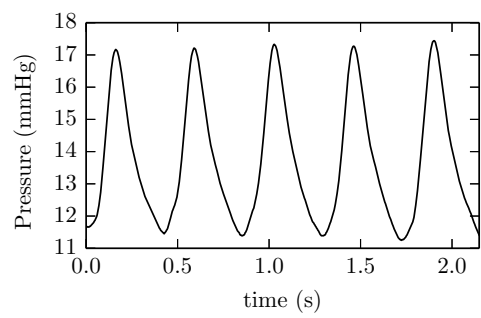
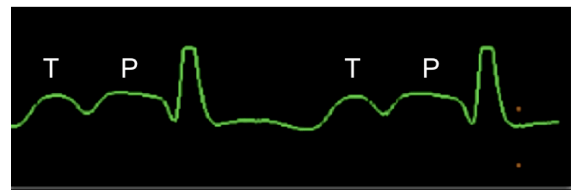


Figure 7: Forward model for patient-B with the estimated parameters: comparison with measurements over two cardiac cycles



(a) Pulmonary venous wedge pressure measurements over 5 cardiac cycles



(b) ECG measurement: the T wave merges with the P wave of next cardiac cycle

Figure 8: Validation measurements for patient-B

Appendix

Details of the haemodynamics measurements. MRIs were acquired on commercially available 1.5T scanners (Philips Intera Achieva, Best, Netherlands; and Siemens Avanto, Siemens Medical Solutions, Erlangen, Germany). A routine pre-stage-II clinical protocol was followed to acquire functional, flow, and three-dimensional information. Free-breathing, electrocardiogram (ECG)-gated velocity-encoded phase contrast imaging sequences were used to acquire flow measurements in multiple locations. Flow measurements were calculated using an in-house plug-in for OsiriX open-source software (OsiriX Foundation, Geneva, Switzerland). A contrast-enhanced three-dimensional angiogram was acquired following administration of 0.2mmol/kg gadoteridol. Cardiac catheterization followed a routine clinical protocol and occurred under general anaesthesia in a bi-plane fluoroscopy suite (Siemens Medical Solutions USA, Inc. Pennsylvania). A fluid-filled catheter system was used to acquire pressure traces and haemodynamic measurements in various systemic and pulmonary arterial and venous locations. Routine echocardiography assessed ventricular and AV valve function; and acquired pulse wave Doppler velocimetry in multiple locations.

References

- Arbia, G., Corsini, C., Baker, C., Pennati, G., Hsia, T.-Y., Vignon-Clementel, I., 2015. Pulmonary hemodynamics simulations before stage 2 single ventricle surgery: Patient-specific parameter identification and clinical data assessment. *Cardiovascular Engineering and Technology*, 1–13.
- Arts, T., Bovendeerd, P., Delhaas, T., Prinzen, F., 2003. Modeling the relation between cardiac pump function and myofiber mechanics. *Journal of biomechanics* 36 (5), 731–736.
- Arts, T., Bovendeerd, P., Prinzen, F. W., Reneman, R. S., 1991. Relation between left ventricular cavity pressure and volume and systolic fiber stress and strain in the wall. *Biophysical journal* 59 (1), 93–102.
- Baretta, A., Corsini, C., Yang, W., Vignon-Clementel, I. E., Marsden, A. L., Feinstein, J. A., Hsia, T.-Y., Dubini, G., Migliavacca, F., Pennati, G., Others, 2011. Virtual surgeries in patients with congenital heart disease: a multi-scale modelling test case. *Philosophical Transactions of the Royal Society A: Mathematical, Physical and Engineering Sciences* 369 (1954), 4316–4330.
- Bellman, R., Bellman, R. E., Bellman, R. E., Bellman, R. E., 1961. *Adaptive control processes: a guided tour*. Vol. 4. Princeton university press Princeton.
- Berne, R. M., Levy, M. N., 1967. *Cardiovascular physiology*. Mosby.
- Bertagna, L., DELia, M., Perego, M., Veneziani, A., 2014. Data assimilation in cardiovascular fluid–structure interaction problems: An introduction. In: *Fluid-Structure Interaction and Biomedical Applications*. Springer, pp. 395–481.
- Bertoglio, C., Moireau, P., Gerbeau, J.-F., 2012. Sequential parameter estimation for fluid–structure problems: Application to hemodynamics. *International Journal for Numerical Methods in Biomedical Engineering* 28 (4), 434–455.
- Beyar, R., Sideman, S., 1984. A computer study of the left ventricular performance based on fiber structure, sarcomere dynamics, and transmural electrical propagation velocity. *Circulation research* 55 (3), 358–375.
- Bovendeerd, P., Borsje, P., Arts, T., van De Vosse, F., 2006. Dependence of intramyocardial pressure and coronary flow on ventricular loading and contractility: a model study. *Annals of biomedical engineering* 34 (12), 1833–1845.
- Caruel, M., Chabiniok, R., Moireau, P., Lecarpentier, Y., Chapelle, D., 2014. Dimensional reductions of a cardiac model for effective validation and calibration. *Biomechanics and modeling in mechanobiology* 13 (4), 897–914.
- Corsini, C., Baker, C., Kung, E., Schievano, S., Arbia, G., Baretta, A., Biglino, G., Migliavacca, F., Dubini, G., Pennati, G., et al., 2014. An integrated approach to patient-specific predictive modeling for single ventricle heart palliation. *Computer methods in biomechanics and biomedical engineering* 17 (14), 1572–1589.
- Corsini, C., Cosentino, D., Pennati, G., Dubini, G., Hsia, T.-Y., Migliavacca, F., 2011. Multiscale models of the hybrid palliation for hypoplastic left heart syndrome. *Journal of biomechanics* 44 (4), 767–770.
- Hann, C., Chase, J., Shaw, G., Smith, B. W., 2004. Identification of patient specific parameters for a minimal cardiac model. In: *Engineering in Medicine and Biology Society, 2004. IEMBS'04. 26th Annual International Conference of the IEEE*. Vol. 1. IEEE, pp. 813–816.
- Hann, C. E., Chase, J. G., Desaive, T., Froissart, C., Revie, J., Stevenson, D., Lambermont, B., Ghuysen, A., Kolh, P., Shaw, G. M., 2010. Unique parameter identification for cardiac diagnosis in critical care using minimal data sets. *Computer methods and programs in biomedicine* 99 (1), 75–87.
- Hann, C. E., Revie, J., Stevenson, D., Heldmann, S., Desaive, T., Froissart, C., Lambermont, B., Ghuysen, A., Kolh, P., Shaw, G. M., et al., 2011. Patient specific identification of the cardiac driver function in a cardiovascular system model. *Computer methods and programs in biomedicine* 101 (2), 201–207.
- Honjo, O., Atlin, C. R., Mertens, L., Al-Radi, O. O., Redington, A. N., Caldarone, C. A., Van Arsdell, G. S., 2011a. Atrioventricular valve repair in patients with functional single-ventricle physiology: impact of ventricular and valve function and morphology on survival and reintervention. *The Journal of thoracic and cardiovascular surgery* 142 (2), 326–335.
- Honjo, O., Mertens, L., Van Arsdell, G. S., 2011b. Atrioventricular valve repair in patients with single-ventricle physiology: mechanisms, techniques of repair, and clinical outcomes. In: *Seminars in Thoracic and Cardiovascular Surgery: Pediatric Cardiac Surgery Annual*. Vol. 14. Elsevier, pp. 75–84.

- Ismail, M., Wall, W. A., Gee, M. W., 2012. Adjoint-based inverse analysis of windkessel parameters for patient-specific vascular models. *Journal of Computational Physics* 244, 113–130.
- Korakianitis, T., Shi, Y., 2006. Numerical simulation of cardiovascular dynamics with healthy and diseased heart valves. *Journal of biomechanics* 39 (11), 1964–1982.
- Migliavacca, F., Dubini, G., Pennati, G., Pietrabissa, R., Fumero, R., Hsia, T.-Y., de Leval, M. R., 2000. Computational model of the fluid dynamics in systemic-to-pulmonary shunts. *Journal of biomechanics* 33 (5), 549–557.
- Moireau, P., Bertoglio, C., Xiao, N., Figueroa, C., Taylor, C., Chappelle, D., Gerbeau, J.-F., 2012. Sequential identification of boundary support parameters in a fluid-structure vascular model using patient image data. *Biomechanics and Modeling in Mechanobiology*, 1–22.
- Moskowitz, S. E., 1982. Passive stress-strain relation for the right ventricle in diastole. *Journal of biomechanics* 15 (4), 249–255.
- Mynard, J., Davidson, M., Penny, D., Smolich, J., 2012. A simple, versatile valve model for use in lumped parameter and one-dimensional cardiovascular models. *International Journal for Numerical Methods in Biomedical Engineering* 28 (6-7), 626–641.
- Paeme, S., Moorhead, K. T., Chase, J. G., Lambermont, B., Kolh, P., D’orio, V., Pierard, L., Moonen, M., Lancellotti, P., Dauby, P. C., et al., 2011. Mathematical multi-scale model of the cardiovascular system including mitral valve dynamics. application to ischemic mitral insufficiency. *Biomed Eng Online* 10 (1), 86.
- Pant, S., Fabrèges, B., Gerbeau, J.-F., Vignon-Clementel, I., 2014. A methodological paradigm for patient-specific multi-scale cfd simulations: from clinical measurements to parameter estimates for individual analysis. *International journal for numerical methods in biomedical engineering* 30 (12), 1614–1648.
- Revie, J. A., Stevenson, D. J., Chase, J. G., Hann, C. E., Lambermont, B. C., Ghuysen, A., Kolh, P., Shaw, G. M., Heldmann, S., Desai, T., 2013. Validation of subject-specific cardiovascular system models from porcine measurements. *Computer methods and programs in biomedicine* 109 (2), 197–210.
- Segal, J., Lerner, D. J., Craig Miller, D., Scott Mitchell, R., Alderman, E. A., Popp, R. L., 1987. When should doppler-determined valve area be better than the gorlin formula?: Variation in hydraulic constants in low flow states. *Journal of the American College of Cardiology* 9 (6), 1294–1305.
- Segers, P., Rietzschel, E., De Buyzere, M., Stergiopoulos, N., Westerhof, N., Van Bortel, L., Gillebert, T., Verdonck, P., 2008. Three-and four-element windkessel models: assessment of their fitting performance in a large cohort of healthy middle-aged individuals. *Proceedings of the Institution of Mechanical Engineers, Part H: Journal of Engineering in Medicine* 222 (4), 417–428.
- Shi, Y., Lawford, P., Hose, R., 2011. Review of zero-d and 1-d models of blood flow in the cardiovascular system. *Biomed Eng Online* 10 (33).
- Shimizu, S., Shishido, T., Une, D., Kamiya, A., Kawada, T., Sano, S., Sugimachi, M., 2010. Right ventricular stiffness constant as a predictor of postoperative hemodynamics in patients with hypoplastic right ventricle: a theoretical analysis. *The Journal of Physiological Sciences* 60 (3), 205–212.
- Spilker, R. L., Taylor, C. a., Aug. 2010. Tuning multidomain hemodynamic simulations to match physiological measurements. *Annals of biomedical engineering* 38 (8), 2635–48.
- Sugimoto, K., Liang, F., Takahara, Y., Mogi, K., Yamazaki, K., Takagi, S., Liu, H., 2013. Assessment of cardiovascular function by combining clinical data with a computational model of the cardiovascular system. *The Journal of thoracic and cardiovascular surgery* 145 (5), 1367–1372.
- Sun, Y., Sjoberg, B., Ask, P., Loyd, D., Wranne, B., 1995. Mathematical model that characterizes transmitral and pulmonary venous flow velocity patterns. *American Journal of Physiology-Heart and Circulatory Physiology* 268 (1), H476–H489.
- Troianowski, G., Taylor, C. A., Feinstein, J. A., Vignon-Clementel, I. E., Others, 2011. Three-dimensional simulations in Glenn patients: clinically based boundary conditions, hemodynamic results and sensitivity to input data. *Transactions of the ASME-K-Journal of Biomechanical Engineering* 133 (11), 111006.
- Vignon-Clementel, I. E., Marsden, A. L., Feinstein, J. A., 2010. A primer on computational simulation in congenital heart disease for the clinician. *Progress in Pediatric Cardiology* 30 (1), 3–13.
- Xiao, N., Alastruey, J., Alberto Figueroa, C., 2013. A systematic comparison between 1-D and 3-D hemodynamics in compliant arterial models. *International journal for numerical methods in biomedical engineering*.